

## BAYESIAN ANALYSIS OF THE LOW-RESOLUTION POLARIZED 3-YEAR WMAP SKY MAPS

H. K. ERIKSEN<sup>1,2,3</sup>, GREG HUEY<sup>4,5,6</sup>, A. J. BANDAY<sup>7</sup>, K. M. GÓRSKI<sup>5,6,8</sup>, J. B. JEWELL<sup>4,5</sup>,  
I. J. O'DWYER<sup>4,5</sup>, B. D. WANDELT<sup>4,7,9</sup>

(Dated: Received - / Accepted -)  
*Draft version February 8, 2022*

### ABSTRACT

We apply a previously developed Gibbs sampling framework to the foreground corrected 3-yr WMAP polarization data and compute the power spectrum and residual foreground template amplitude posterior distributions. We first analyze the co-added Q- and V-band data, and compare our results to the likelihood code published by the WMAP team. We find good agreement, and thus verify the numerics and data processing steps of both approaches. However, we also analyze the Q- and V-band separately, allowing for non-zero EB cross-correlations and including two individual foreground template amplitudes tracing synchrotron and dust emission. In these analyses, we find tentative evidence of systematics: The foreground tracers correlate with each of the Q- and V-band sky maps individually, although not with the co-added QV map; there is a noticeable negative EB cross-correlation at  $\ell \gtrsim 16$  in the V-band map; and finally, when relaxing the constraints on EB and BB, noticeable differences are observed between the marginalized band powers in the Q- and V-bands. Further studies of these features are imperative, given the importance of the low- $\ell$  EE spectrum on the optical depth of reionization  $\tau$  and the spectral index of scalar perturbations  $n_s$ .

*Subject headings:* cosmic microwave background — cosmology: observations — methods: numerical

### 1. INTRODUCTION

One of the most remarkable results in the 3-yr data release from the Wilkinson Microwave Anisotropy Probe (WMAP) experiment (Hinshaw et al. 2007; Page et al. 2007) was the detection of large-scale E-mode polarization at millimeter wavelengths. This was interpreted as the theoretically predicted signature of reionization, and allowed the WMAP team to set new and tighter constraints on the optical depth of reionization  $\tau$ . In turn, the well-known degeneracy between  $\tau$  and the spectral index of primordial scalar perturbations  $n_s$  was broken. The final outcome was a claimed detection of  $n_s \neq 1$  at a statistical significance of almost  $3\sigma$  (Spergel et al. 2007).

One should bear in mind, however, the great potential for systematics effects in both the temperature and polarization measurements. For instance, the precise level of power contribution from unresolved point sources affects  $n_s$  directly. An independent analysis of this particular issue by Huffenberger et al. (2006) showed that the initial point source amplitude quoted by the WMAP team was indeed too high, which biased  $n_s$  to low values. Similarly, on large scales the likelihood approximation used by the WMAP team was biased high (Eriksen et al. 2007), which also biased  $n_s$  low. After these corrections,

the statistical significance of  $n_s \neq 1$  dropped to  $\sim 2\sigma$ .

For polarization the situation may be even more serious due to the strong sensitivity of  $\tau$  and  $n_s$  on the low- $\ell$  EE spectrum, combined with the low signal-to-noise ratio of the WMAP data. Systematic effects, both from the instrument itself (Jarosik et al. 2007) and from non-cosmological foregrounds (Kogut et al. 2007), are much more likely to affect the results, and we are also much less likely to detect them. It is therefore imperative to carefully check both the data and the analysis methods, in order to build up confidence in the final cosmological results. In this Letter, we start this task by computing the low- $\ell$  EE, EB, BB and foreground template amplitude posterior distributions from the WMAP data.

### 2. METHOD

We use a previously introduced Gibbs sampling framework (Jewell et al. 2004, Wandelt et al. 2004, Eriksen et al. 2004, Larson et al. 2007; hereafter JWEL) to estimate the posterior distributions. For full details on the method, we refer the interested reader to the quoted papers, and only summarize the principles here.

First we define our notation. The desired distribution is denoted  $P(\mathbf{s}, C_\ell, \mathbf{f}|\mathbf{d})$ , where  $\mathbf{s}$  is the CMB signal,  $C_\ell = \{C_\ell^{EE}, C_\ell^{EB}, C_\ell^{BB}\}$  is the CMB power spectrum,  $\mathbf{f}$  is a set of foreground template amplitudes, and  $\mathbf{d}$  are the data.

The Gibbs sampler is a Markov Chain Monte Carlo method, and, as such, maps out the full posterior by drawing samples from it. While direct evaluation or sampling from the posterior  $P(C_\ell|\mathbf{d})$  requires inversion of a prohibitively large matrix, the Gibbs sampling scheme (Gelfand & Smith 1990) uses the conditional densities of the joint posterior  $P(C_\ell, \mathbf{s}|\mathbf{d})$  which is computationally feasible to sample from. The algorithm may thus be de-

<sup>1</sup> email: h.k.k.eriksen@astro.uio.no

<sup>2</sup> Institute of Theoretical Astrophysics, University of Oslo, P.O. Box 1029 Blindern, N-0315 Oslo, Norway

<sup>3</sup> Centre of Mathematics for Applications, University of Oslo, P.O. Box 1053 Blindern, N-0316 Oslo

<sup>4</sup> Department of Physics, University of Illinois, Urbana, IL 61801

<sup>5</sup> Jet Propulsion Laboratory, 4800 Oak Grove Drive, Pasadena CA 91109

<sup>6</sup> California Institute of Technology, Pasadena, CA 91125

<sup>7</sup> Max-Planck-Institut für Astrophysik, Karl-Schwarzschild-Str. 1, Postfach 1317, D-85741 Garching bei München, Germany

<sup>8</sup> Warsaw University Observatory, Aleje Ujazdowskie 4, 00-478 Warszawa, Poland

<sup>9</sup> Astronomy Department, University of Illinois at Urbana-Champaign, IL 61801-3080

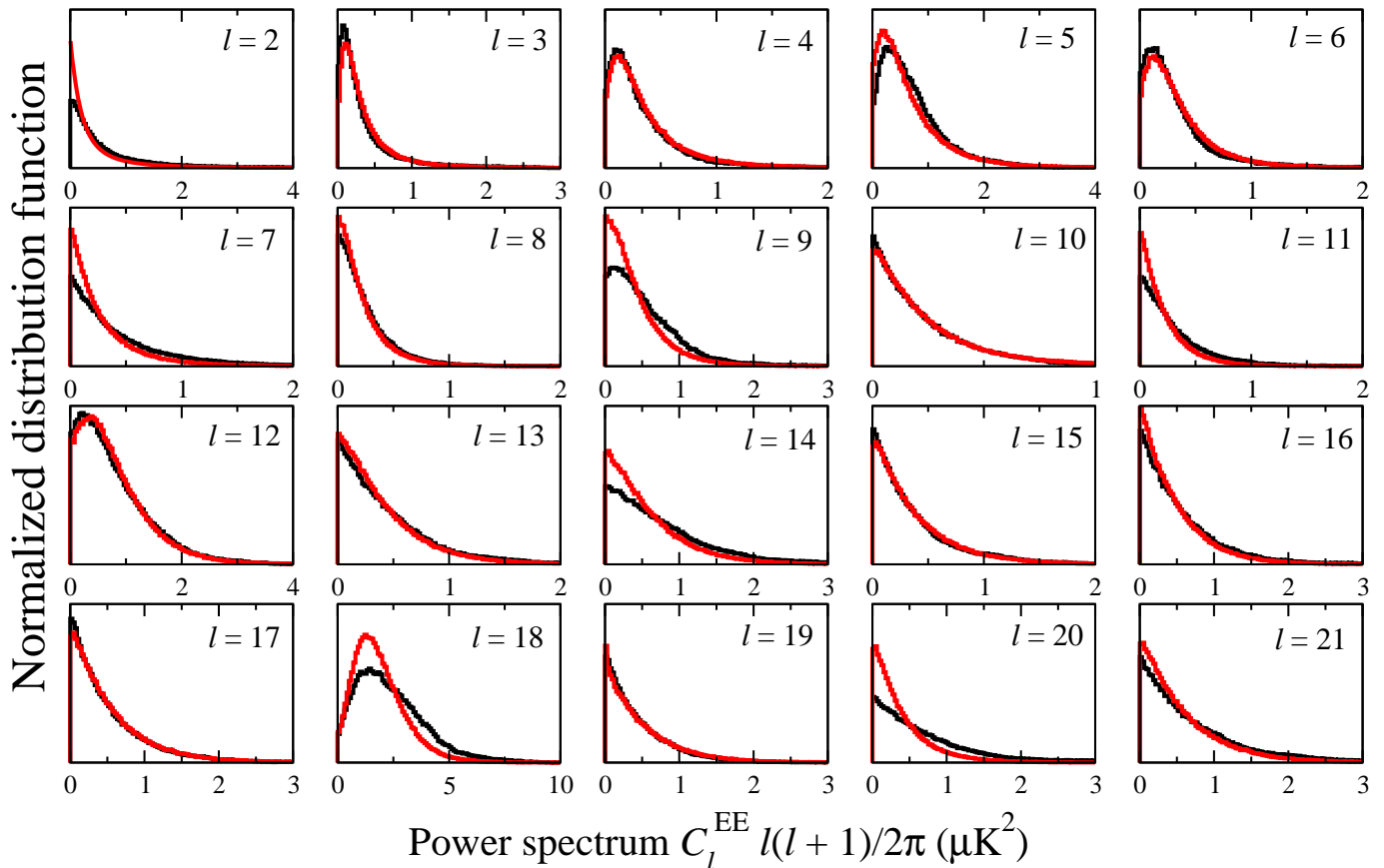


FIG. 1.— Comparison of single- $\ell$  EE marginal posteriors from the WMAP code (black distributions) and the Gibbs sampler (red distributions) using the QV map. The EB and BB power spectra are held at zero.

scribed by the following sampling steps,

$$\mathbf{s}^{i+1} \leftarrow P(\mathbf{s} | C_\ell^i, \mathbf{f}^i, \mathbf{d}) \quad (1)$$

$$C_\ell^{i+1} \leftarrow P(C_\ell | \mathbf{s}^{i+1}, \mathbf{f}^i, \mathbf{d}) \quad (2)$$

$$\mathbf{f}^{i+1} \leftarrow P(\mathbf{f} | \mathbf{s}^{i+1}, C_\ell^{i+1}, \mathbf{d}). \quad (3)$$

Here the symbol  $\leftarrow$  indicates sampling from the conditional distribution on the right hand side, which can be accomplished without inverting the signal-plus-noise covariance matrix (see JWEL for details). For the foreground template amplitude distribution, we note that the required algorithm is identical to that employed for sampling monopole and dipole amplitudes (Eriksen et al. 2004).

### 3. DATA

We consider only the low-resolution foreground-corrected 3-yr WMAP polarization data in this Letter, as provided on LAMBDA<sup>10</sup>. These come in the form of three HEALPix<sup>11</sup> sky maps, pixelized at  $N_{\text{side}} = 16$ , each having 3072 pixels in both Stoke's Q and U. The WMAP P06 sky cut is imposed on the data, leaving only 2267 pixels for the analysis. Two frequency bands are included, namely Q-band (41 GHz) and V-band (61 GHz). In addition, we analyze the co-added map (denoted QV), and also the two frequency maps jointly but not co-added (denoted Q+V). All maps are provided with a full noise co-

variance matrix (Jarosik et al. 2007), appropriately corrected for the P06 sky cut and removal of foreground templates. The units used in this paper are thermodynamic  $\mu\text{K}$ .

For foreground marginalization, we adopt two individual templates. First, we use the K–Ka difference map, smoothed to  $10^\circ$  FWHM resolution to reduce noise contributions, as a tracer of synchrotron emission. Second, for dust emission we adopt the low-noise template developed by the WMAP team for their foreground correction procedure (Page et al. 2007). Note that the specific shape of these templates are of minor importance; if the provided sky maps are free of foregrounds, they should not correlate significantly with any non-CMB map.

We compare our results to the official WMAP likelihood code<sup>12</sup>, also available from LAMBDA. To map out the appropriate posteriors, we have written a special-purpose MCMC wrapper around this likelihood code.

### 4. RESULTS

#### 4.1. Numerical verification of the WMAP likelihood

The first case considered is that adopted by the WMAP likelihood code, namely the co-added QV map. For this analysis, we fix the EB and BB spectra to zero, and map out the corresponding marginalized EE posteriors  $\ell$ -by- $\ell$ , both with the Gibbs sampler and by the WMAP-based MCMC code.

The results from this exercise are shown in Figure 1.

<sup>10</sup> <http://lambda.gsfc.nasa.gov>

<sup>11</sup> <http://healpix.jpl.nasa.gov>

<sup>12</sup> version v2p2p2

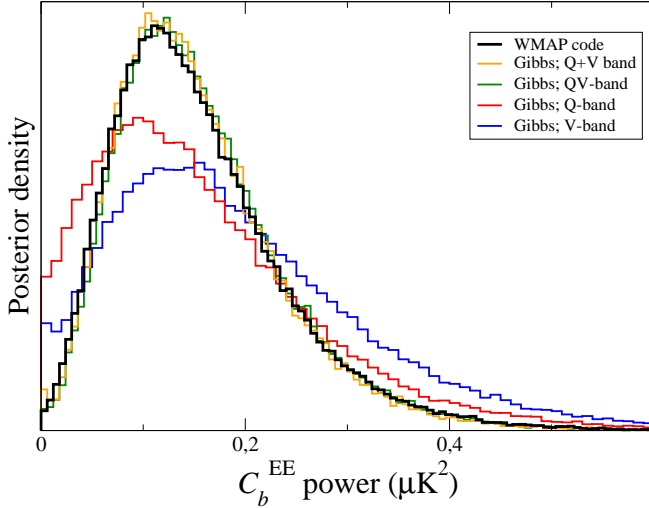


FIG. 2.— Marginal posterior distributions for the EE bin power between  $\ell = 2-6$ .

The agreement between the two approaches is very good, and this is an important validation of the WMAP data processing method: First, we analyze the data at their native  $N_{\text{side}} = 16$  resolution, while the WMAP team analyze maps downgraded to  $N_{\text{side}} = 8$ . Second, they marginalize over a single total foreground template, while we marginalize over the K–Ka difference map and a dust template. Third, we use a Gibbs sampler for the numerical work, while the WMAP team uses a brute-force likelihood evaluator. None of these differences affects the low- $\ell$  EE spectrum peak visibly, as will be quantified more precisely in the next section.

#### 4.2. Generalized analysis

Having validated the numerics and data processing steps in both procedures, we now expand the analysis and allow for non-zero EB and/or BB spectra. We also compute the posteriors for each frequency band separately and jointly. For presentational reasons, we report only band powers in EE and BB between  $\ell = 2-6$  and  $\ell = 2-20$ , respectively. Cases of special interest are treated separately in subsequent sections.

In order to achieve good convergence,  $10^6$  samples were generated for the non-zero EB,  $\ell = 2-20$  cases. For all other cases,  $10^5$  samples were generated. The CPU time to generate one sample was  $\sim 2$  seconds.

The results from these computations are summarized in Table 1. The EE posteriors with fixed EB = BB = 0 are shown in Figure 2. Again, note the excellent agreement between the WMAP results and the QV and Q+V cases in the two top sections.

However, even though the joint QV analyses agree well, the picture is considerably less clear when it comes to single bands and relaxed EB constraints. On the one hand, there appears to be more EE power in the V-band data than in the Q-band data. On the other hand, there may seem to be small traces of BB power in the Q-band data.

The BB posteriors develop a peak away from  $C_\ell^{\text{BB}} = 0$  in the EB  $\neq 0$  case. This is not surprising. Since the signal covariance matrix is positive definite, one must have  $C_\ell^{\text{EE}} C_\ell^{\text{BB}} > (C_\ell^{\text{EB}})^2$ . Therefore, when marginalizing over  $C_\ell^{\text{EB}}$ , a non-zero peak emerges in both the EE and

TABLE 1  
MARGINALIZED EE AND BB BAND POWERS

| Data set             | EE power ( $10^{-1} \mu\text{K}^2$ ) |                        | BB power ( $10^{-1} \mu\text{K}^2$ ) |                     |
|----------------------|--------------------------------------|------------------------|--------------------------------------|---------------------|
|                      | $\ell = 2-6$                         | $\ell = 2-20$          | $\ell = 2-6$                         | $\ell = 2-20$       |
| EE free; EB = BB = 0 |                                      |                        |                                      |                     |
| WMAP                 | $1.1^{+0.9}_{-0.5}$                  | $0.64^{+0.46}_{-0.34}$ | ...                                  | ...                 |
| QV-band              | $1.2^{+0.9}_{-0.6}$                  | $0.67^{+0.39}_{-0.38}$ | ...                                  | ...                 |
| Q+V-band             | $1.1^{+0.8}_{-0.6}$                  | $0.65^{+0.38}_{-0.35}$ | ...                                  | ...                 |
| Q-band               | $1.0^{+1.0}_{-0.8}$                  | $0.36^{+0.67}_{-0.36}$ | ...                                  | ...                 |
| V-band               | $1.3^{+1.2}_{-0.9}$                  | $1.2^{+0.9}_{-0.7}$    | ...                                  | ...                 |
| EE, BB free; EB = 0  |                                      |                        |                                      |                     |
| WMAP                 | $0.94^{+0.76}_{-0.58}$               | $0.63^{+0.44}_{-0.37}$ | $< 0.70$                             | $< 0.40$            |
| QV-band              | $1.1^{+0.8}_{-0.6}$                  | $0.61^{+0.38}_{-0.37}$ | $< 0.57$                             | $< 0.26$            |
| Q+V-band             | $1.1^{+0.8}_{-0.6}$                  | $0.57^{+0.40}_{-0.31}$ | $< 0.58$                             | $< 0.30$            |
| Q-band               | $0.3^{+1.3}_{-0.3}$                  | $0.23^{+0.68}_{-0.23}$ | $0.3^{+1.2}_{-0.2}$                  | $< 0.71$            |
| V-band               | $1.4^{+1.4}_{-0.9}$                  | $1.1^{+1.0}_{-0.7}$    | $< 0.94$                             | $< 0.51$            |
| EE, EB, BB free      |                                      |                        |                                      |                     |
| QV-band              | $1.4^{+0.9}_{-0.7}$                  | $0.65^{+0.41}_{-0.30}$ | $0.30^{+0.60}_{-0.30}$               | $0.1^{+0.3}_{-0.1}$ |
| Q+V-band             | $1.3^{+0.9}_{-0.7}$                  | $0.66^{+0.43}_{-0.30}$ | $0.31^{+0.59}_{-0.31}$               | $0.1^{+0.3}_{-0.1}$ |
| Q-band               | $1.1^{+1.1}_{-0.8}$                  | $0.54^{+0.65}_{-0.36}$ | $0.7^{+1.3}_{-0.6}$                  | $0.5^{+0.7}_{-0.4}$ |
| V-band               | $1.8^{+1.6}_{-1.1}$                  | $1.5^{+0.9}_{-0.9}$    | $0.47^{+0.93}_{-0.47}$               | $0.4^{+0.6}_{-0.4}$ |

NOTE. — Values indicate either the posterior mode and upper and lower 68% confidence interval, or the upper 68% confidence limits. If the lower error bar equals the posterior mode value, a non-zero peak is detected, but at a significance of less than 68%.

BB spectra individually.

##### 4.2.1. Foreground amplitude posteriors

In Figure 3 we show the foreground template amplitude posteriors for the Q-, V- and QV-band data, for the case with fixed EB = BB = 0. Although no signs of significant residual foregrounds are observed in the co-added QV band, apparently confirming the fits made by the WMAP team, the same is not true for each band individually. On the contrary, non-zero correlations are seen in both the Q- and V-band data individually.

For the Q-band data, the marginal best-fit K–Ka amplitude is  $A_s = -0.027^{+0.014}_{-0.17}$ , different from zero at  $2\sigma$ . The best-fit dust amplitude is  $A_d = 15.7^{+8.7}_{-10.7}$ . For the V-band data, the best-fit dust amplitude is  $A_d = -24.1^{+10.3}_{-11.3}$ ,  $2.3\sigma$  away from zero. The K–Ka amplitude is  $A_s = 0.011^{+0.015}_{-0.018}$ .

These results may be compared to Table 4 of Page et al. (2007). The main difference between the two analyses is that while we apply the conservative P06 mask to the data, Page et al. (2007) apply the much more aggressive processing mask described by Jarosik et al. (2007). The two analyses remove 26.4% and 5.7% of the sky, respectively. Considering that all cosmological analyses are carried out with the P06 mask, and that variations in the synchrotron spectral index are observed between the galactic plane and the high latitudes (Kogut et al. 2007), it is not immediately clear to us why the more aggressive mask was chosen for this task by the WMAP team. The improvement in raw  $\chi^2$  after further correcting the “cleaned” WMAP maps for these residuals

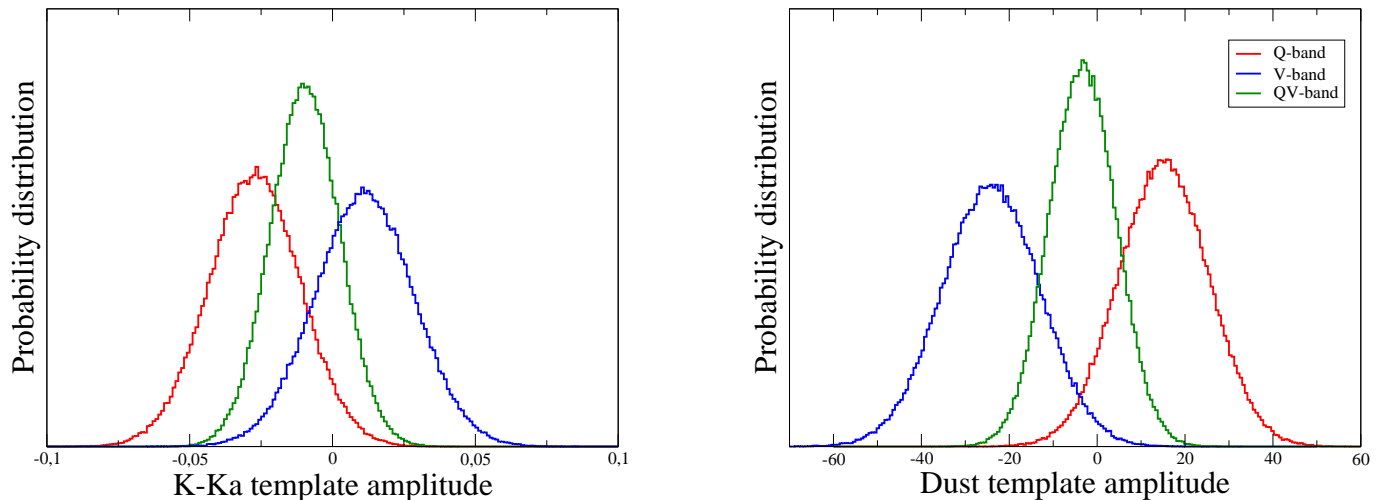


FIG. 3.— The foreground template amplitude marginal posteriors for the Q-, V- and QV-bands. For this plot, the EB and BB power spectra were set to zero.

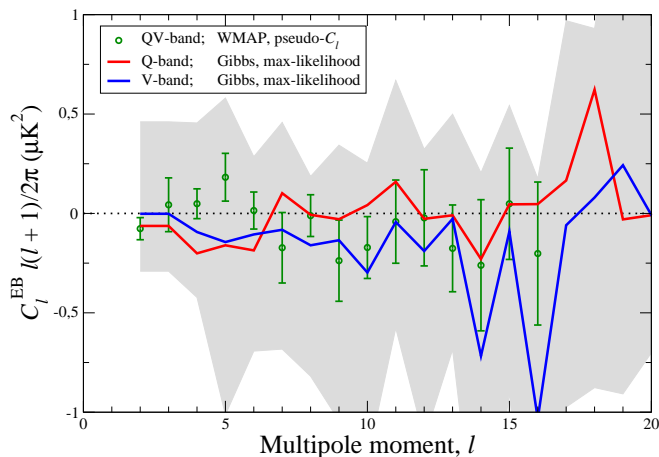


FIG. 4.— The E $\times$ B cross-power spectrum. The gray region shows the  $1\sigma$  confidence region around the V-band spectrum (blue curve); note that the marginal EB posterior is strongly non-Gaussian with heavy tails. The green data points show the WMAP EB spectrum computed with a pseudo- $C_\ell$  estimator with Gaussian error bars. is  $-5.4$  for the Q-band and  $-3.3$  for the V-band, respectively.

Two other, minor differences are that we take into account both the full noise and CMB covariance matrices, while the WMAP team includes only a white noise covariance approximation. Note that this carries no extra cost within the Gibbs sampling framework.

#### 4.2.2. E $\times$ B cross-correlation spectra

We find evidence for a non-zero EB correlation in the V-band sky map. This spectrum is shown in Figure 4 for the Q- and V-band sky maps individually, together with the pseudo- $C_\ell$  EB QV-band spectrum computed by the WMAP team. Note the consistently negative correlation observed in the V-band. Although the significance of the negative correlation is not more than a few tenths per multipole, and the joint significance is not more than 1 to  $2\sigma$  depending on binning scheme, it is observed consistently in every multipole up to  $\ell = 17$ . A similar, though weaker, trend is seen in the pseudo-spectrum computed by the WMAP team from the QV combination.

## 5. CONCLUSIONS

We have performed a Bayesian analysis of the low-resolution foreground-corrected 3-yr WMAP polarization data using a previously described methodology based on the Gibbs sampler. By doing so, we validated the numerical implementation of the official WMAP likelihood code, as well as their procedure for degradation of map resolution. However, when generalizing the analysis to allow for non-zero EB and BB power spectrum components, and also considering individual frequency bands, we found several issues that may be important for the cosmological interpretation of these data.

First and foremost, when relaxing the constraints on EB and BB, noticeable differences between the Q- and V-band posteriors are observed. Specifically, we find generally more EE power in the V-band data than in the Q-band data, but also perhaps some hints of BB power in the Q-band data. At the same time, we have also found a negative EB correlation in the V-band map, as well as residual foregrounds in both maps.

If these tentative findings are confirmed by future experiments or additional years of WMAP observations, significant shifts in cosmological parameters could be the result. For example, if the V-band data alone were used for the WMAP3 analysis instead of the QV combination, the amplitude of the  $\ell = 2-6$  EE detection would increase by 20–50%, depending on whether BB is allowed to vary or not. Consequently,  $\tau$  could increase from 0.09 to  $\sim 0.12$ , and  $n_s$  by a percent or two, comparable to its current nominal statistical uncertainty of 0.015, from  $\sim 0.97$  to  $\sim 0.98$ .

As discussed in the introduction, systematics are a serious concern for both the temperature and polarization data for both  $\tau$  and  $n_s$ . It is important to bear in mind that the currently quoted uncertainties on these quantities often found in the literature are statistical only. The unknown systematic uncertainties may turn out to be non-negligible for the currently available data sets, and, in particular, we believe it is too early to draw any firm conclusions concerning the precise value of  $n_s$ . Fortunately, Planck will clarify these issues in the near future.

We wish to thank David Larson for his contributions during the early phases of this project. We acknowl-

edge use of the Legacy Archive for Microwave Background Data Analysis (LAMBDA). We acknowledge use of the HEALPix software (Górski et al. 2005) and analysis package for deriving the results in this paper. This work was partially performed at the Jet Propulsion Laboratory, California Institute of Technology, under a con-

tract with the National Aeronautics and Space Administration. HKE acknowledges financial support from the Research Council of Norway. BDW acknowledges support by NSF grant no. 0507676, the Friedrich Wilhelm Bessel Research Prize by the Alexander v. Humboldt foundation and NASA subcontract no. 1236748.

#### REFERENCES

- Eriksen, H. K., et al. 2004, *ApJS*, 155, 227  
 Eriksen, H. K., et al. 2007, *ApJ*, 641, 665  
 Gelfand, A. E., & Smith, A. F. M. 1990, *J. Am. Stat. Asso.*, 85, 398  
 Górski, K. M., Hivon, E., Banday, A. J., Wandelt, B. D., Hansen, F. K., Reinecke, M., & Bartelmann, M. 2005, *ApJ*, 622, 759  
 Hinshaw, G., et al. 2007, *ApJ*, in press [astro-ph/0603451]  
 Huffenberger, K. M., Eriksen, H. K., & Hansen, F. K. 2006, *ApJ*, 651, L81  
 Jarosik, N., et al. 2007, *ApJ*, in press, [astro-ph/0603452]  
 Jewell, J., Levin, S., & Anderson, C. H. 2004, *ApJ*, 609, 1  
 Kogut, A., et al. 2007, *ApJ*, submitted [arXiv:0704.3991]  
 Larson, D. L., Eriksen, H. K., Wandelt, B. D., Górski, K. M., Huey, G., Jewell, J. B., & O'Dwyer, I. J. 2007, *ApJ*, 656, 653  
 Page, L., et al. 2007, *ApJ*, in press, [astro-ph/0603450]  
 Spergel, D. N., et al. 2007, *ApJ*, in press, [astro-ph/0603449]  
 Wandelt, B. D., Larson, D. L., & Lakshminarayanan, A. 2004, *Phys. Rev. D*, 70, 083511